Multilayer-by-multilayer surface melting of Cu(200)

Kai Wang,[1] Haizhen Wu,[2] Mengke Ge,[1] Xingang Hou,[1] Ning Liu,[1] Jia He,[1,*] Wei Xi,[1,†] and Jun Luo[1]

[1]*Center for Electron Microscopy, TUT-FEI Joint Laboratory, Tianjin Key Laboratory of Advanced Functional Porous Materials, Institute for New Energy Materials & Low-Carbon Technologies, School of Materials Science and Engineering, Tianjin University of Technology, Tianjin 300384, China*

[2]*Institute of Material Physics, Key Laboratory of Display Materials and Photoelectric Devices, Ministry of Education, Tianjin University of Technology, Tianjin 300384, China*

(Received 13 March 2018; revised manuscript received 9 July 2018; published 25 July 2018)

It is well known that surface melting of metal materials is caused by vacancies, and melting proceeds layer by layer in theoretical predictions. However, the melting process has rarely been directly investigated in real time at atomic resolution. Herein, the (200) surface-melting process of Cu nanoparticles with sizes of about 50 nm at 750°C was first observed by *in situ* heating transmission electron microscopy. Initially, surface-melting nucleation occurs at the edge and corner of one side of the Cu(200) surface. Subsequently, the nucleated region size increases to a critical value (about 14 layers). Finally, collapse-type melting rapidly extends to the whole Cu(200) surface. This surface-melting process repeatedly occurs. This work will enhance the understanding of the surface-melting mechanism and provide a theoretical foundation to avoid the collapse of Cu nanomaterials during high-temperature applications.

DOI: 10.1103/PhysRevB.98.045425

I. INTRODUCTION

Melting of solids is one of the most common phenomena for phase transitions. However, the mechanism of melting is still an outstanding problem in condensed-matter physics [1,2]. Because nanoscale materials, such as nanoparticles, possess large surface or interface areas, their melting behavior, which greatly differs from that of conventional bulk solids, is complicated. The surfaces of nanomaterials have relatively low thermal stabilities because the surface atoms have lower coordination numbers and unfavorable cohesive energies compared with the internal atoms. Hence, melting is normally initiated at the solid surface or interface [3,4], which is called surface melting.

Since the early 20th century, numerous computer simulations of metal melting have been performed and a few theories have been proposed to explain the surface-melting phenomenon [5,6]. Surface melting of face-centered-cubic (fcc) metals is crystal-face dependent. Moreover, the melting temperature is related to the close-packed surface, which is the same for hexagonal close-packed metals [7]. For example, in fcc metals, the temperature gradually increases to the bulk melting point (T_m). The (111) surface does not melt below T_m or superheat above T_m [8–10], the (100) surface exhibits incomplete surface melting (i.e., the thickness of the surface liquid layer remains finite as the temperature approaches T_m [11–13]), and the (110) surface exhibits complete surface melting [14–19].

Simulation results usually show that the melting behavior of metal surfaces is caused by the existence of vacancies in the crystal face [20,21]. In metal crystals, vacancies are more easily produced in high-index surfaces than in low-index surfaces upon heating, and thus they possess lower melting temperatures. Thus, it can be inferred that when the temperature increases to even hundreds of kelvin lower than T_m, the first layer of these crystal faces starts to produce vacancies, which means that surface melting starts. Vacancies are then produced in the second layer and it melts, and the metal surface melts layer by layer from the outside to the inside. It needs to be pointed out that this inference depends on an infinite surface, while the surfaces of metal nanoparticles usually have edges and cannot be infinite owing to the crystal structure characteristics. Therefore, the process of surface melting of metal nanoparticles may be different from these simulations.

Cu and Cu-based nanomaterials are used in many high-temperature fields and have been widely investigated [22]. The melting point of bulk Cu is 1083°C. Molecular dynamics (MD) simulations show that the melting temperature of Cu nanoparticles with a diameter of 10.8 nm is 650°C [23]. However, experiments show that the melting temperatures of 40 and 50 nm Cu nanoparticles are about 187 and 327°C, respectively [24]. Therefore, research of the surface melting of Cu nanoparticles may provide insight into the surface-melting mechanism and provide a theoretical foundation to avoid high-temperature failure of Cu nanomaterials. In this work, we investigated surface melting of Cu(200) at the atomic scale by *in situ* heating transmission electron microscopy (TEM). The results reveal that the Cu(200) surface melts multilayer by multilayer at 750°C.

II. MATERIALS AND METHODS

Cu nanoparticles with a size of ca. 50 nm were synthesized by ball milling and high-temperature reduction [25]. In brief, pure Cu powder (5 g, 99.99%, 100 mesh) was first treated by

*hejia@tjut.edu.cn
†weiandna1234@163.com

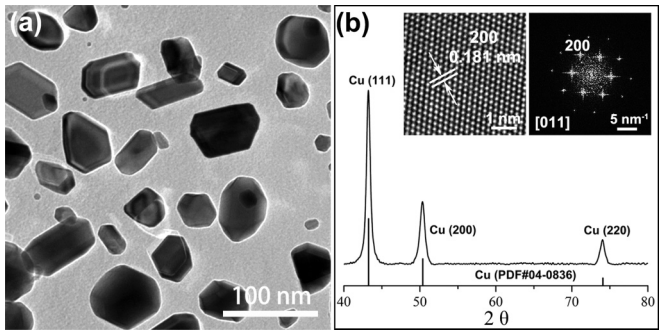

FIG. 1. Morphologies of the Cu nanoparticles at room temperature: (a) TEM bright-field image and (b) x-ray diffraction pattern of a Cu nanoparticle. The insets in (b) are a high-resolution image and the corresponding FFT pattern.

ball milling in 100 ml $CuCl_2$ solution with $[Cl^-] = 0.75 \times 10^2$ mol L^{-1}. The rotating speed of ball milling was 400 rpm and the duration was 25 h. The size of the mill balls was 15 mm and the ball-to-powder weight ratio was 20:1. The as-milled product was rinsed with distilled water and then dried in vacuum at 40°C for 2 h. Finally, Cu nanoparticles were obtained by reducing the resulting products at 400°C for 15 min under ammonia.

For *in situ* observation, the Cu nanoparticles were dispersed on a heating chip (Wildfire S5, DENSsolutions, Netherlands). The heating temperature range was 23–1300°C and the temperature error was <5% [26]. A charge-coupled device (CCD) camera was used to record the melting process of the Cu nanoparticles in high-resolution TEM (HRTEM, Talos F200X) with an acceleration voltage of 200 KV and a heating rate of 30°C/min.

We performed the MD simulations with LAMMPS [27]. The embedded atom method potential was used to describe the interatomic interactions [28]. For the Cu(200) surface, we constructed a cell composed of 50 atomic layers with dimensions of 14.46 × 14.46 × 14.0 nm. Periodic boundary conditions were applied in the three directions of Cartesian space. The bottom 10 layers were fixed during the MD simulations. To simulate the corresponding environment of the corner of the Cu nanoparticle, some of the Cu(200) surface atoms were truncated, as shown in Fig. S1 in the Supplemental Material (SM) [29]. The system was maintained at 1000 K with the constant volume, particle number, and temperature (NVT) ensemble for 1000 ps with a time step of 1 fs. Analysis of the simulations was performed with the Visual Molecular Dynamics (VMD) program [30].

III. RESULTS AND DISCUSSION

The Cu nanoparticles obtained by ball milling and high-temperature reduction have good crystallinity, with an average particle size of about 50 nm. Figure 1(a) shows that the particles have relatively complete surfaces and polyhedral shapes at room temperature. The crystallinity of the Cu nanoparticles was confirmed by x-ray diffraction, and the results are consistent with the theoretical values [Fig. 1(b)]. A high-resolution image of Fig. 1(a) and the corresponding fast Fourier transform

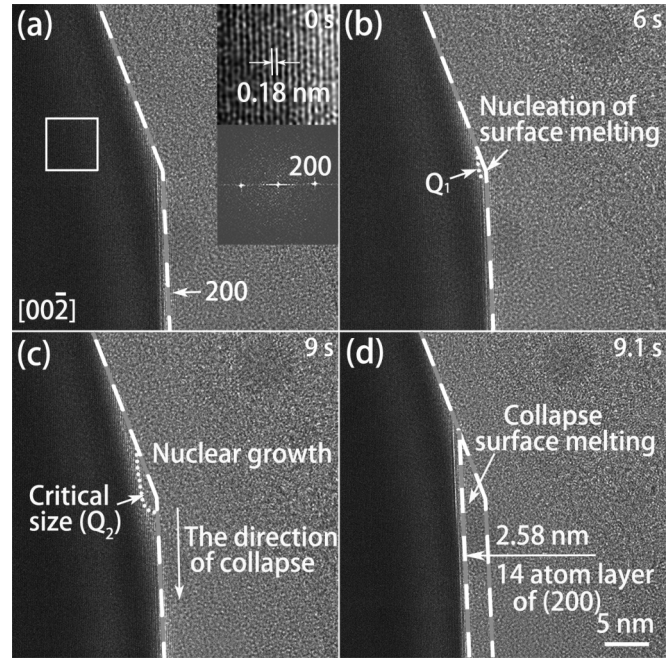

FIG. 2. Surface-melting process of the Cu(200) surface at 750°C. (a)–(d) TEM images of the same area of the Cu nanoparticle showing the melting process of the Cu(200) surface at 0, 6, 9, and 9.1 s, respectively. The inset in (a) is the high-resolution image and the corresponding FFT image, which shows that the crystal orientation is the Cu(200) surface. The scale of the figures is the same (5 nm).

(FFT) image are shown in Fig. 1(b), which are consistent with fcc crystalline Cu.

The surface-melting process of Cu(200) at 750°C was observed by *in situ* TEM (surface melting occurs during the 750°C heat preservation period and the heating curve; see Fig. S2 in the SM [29]). The (100) diffraction spot of the face-centered-cubic structure will not appear owing to systematic extinction, and the (200) spot appears when the microstructure is characterized by the electron diffraction pattern. To avoid confusion, we express it as Cu(200) in this paper. Figure 2 shows typical high-resolution images of the process. This is a partial image of a Cu nanoparticle [Fig. 2(a)] and its enlarged image and the FFT image of the selected area [the box in Fig. 2(a)] show that the particle surface is Cu(200). When the temperature is held at 750°C, the edge atoms that have the lowest coordination number first break away from the crystal lattice and form the nucleation region Q_1 [Fig. 2(b)] [31–33]. This is because the atoms at the corner have low cohesive energy and the bonds are easily broken under heating. When the holding time increases, the nucleation region Q_1 increases to a critical size Q_2 [Fig. 2(c)] (for more details about Q_2, see Fig. S3 in the SM [29]), which is about 2.58 nm thick and contains 14 layers of Cu(200). The interface between Q_2 and the nanoparticle is concave with negative curvature, which reduces the energy of the interface and increases the thermal stability of the solid part [34]. The decrease of the energy restricts the melt along the depth direction, so it instantly melts and collapses along the Cu(200) surface [Fig. 2(d)]. Since 14 surface layers of Cu (200) are simultaneously melted, we call

it multilayer melting in this paper. It should be noted that the sampling interval between Figs. 2(c) and 2(d) is only 0.1 s, which is the CCD camera frequency. The actual time of surface collapse is shorter than 0.1 s [35]. Moreover, collapse forms a new surface and corner and the surface-melting process is continuously repeated.

It is worthwhile to note that the observed surface-melting process is clearly different from the traditional surface-melting mechanism. In theoretical calculations, materials melt layer by layer because vacancies always preferentially form in the outermost layer, and the vacancies are the main origin of melting. However, in our experiment, the origin is the atoms at the corner that have low cohesive energy, rather than vacancies. When an edge and a corner exist, the traditional surface-melting mechanism, which is applicable to the infinite surface, may no longer be suitable for nanoparticles. The surface-melting process we observed (multilayer-by-multilayer melting) can be considered to be another type of gradual melting process. Two videos of the surface-melting process are provided in the Supplemental Material (Videos S1 and S2) [29].

The thermal stability of a metal crystal is related to the cohesive energy [36]. The cohesive energy of Cu nanoparticles is equal to the energy required to break the metal into isolated atoms by destroying all of the metal bonds. Thus, we calculated the cohesive energy of every atom of the Cu nanoparticles to further investigate the surface-melting mechanism.

The cohesive energy of a nanoparticle is the contributions of the internal and external atoms. The internal atoms are the same as the atoms in the bulk material, but the external atoms have dangling bonds, which results in a decrease in the coordination number [37]. Nanoparticles are generally polyhedral [38–40]. The external atoms consist of surface, edge, and corner atoms, as shown in Fig. 1(a). Thus, the relationship between the coordination number C_i and the cohesive energy E of the external atoms can be expressed as

$$\varepsilon_i = \frac{\left[1+\exp\left(\frac{12-C_i}{8C_i}\right)\right]\varepsilon_t}{2}, \tag{1}$$

$$E_i = C_i\varepsilon_i. \tag{2}$$

In this system, E is the cohesive energy of the Cu atom and C is the coordination number of the Cu atom. The cohesive energy of one atom can be simplified to be only related to the metallic bonds with nearest-neighbor atoms [41]. Here, i is the index of the coordination number ($i = 4$, 5, 6, 8, and 12), ε_t is the bond strength (BS) of the bulk atoms, and ε_i are the BSs of the surface, edge, and corner atoms.

We calculated the cohesive energies of the edge and corner atoms using Eqs. (1) and (2). The coordination numbers at the edge and corner are mainly $C_i = 4$, 5, 6, and 8, and the coordination numbers of the internal atoms are greater than 8. Figure 3(a) shows the distribution of C_i at the edge and corner and sets the model surface to interface. The cohesive energies E_i corresponding to C_i are approximately $E_4 = 3.36\varepsilon_t$, $E_5 = 3.69\varepsilon_t$, $E_6 = 4.02\varepsilon_t$, $E_8 = 4.68\varepsilon_t$, and $E_{12} = 12\varepsilon_t$. The coordination number of the atoms in the infinite Cu(200) surface is 8. Thus, the cohesive energies of the edge and corner atoms are significantly lower than that of the Cu(200) surface because $C_i < 8$. Therefore, separation of the atoms at the edge and corner is easier than at the infinite surface, leading to surface melting beginning at the edge and corner.

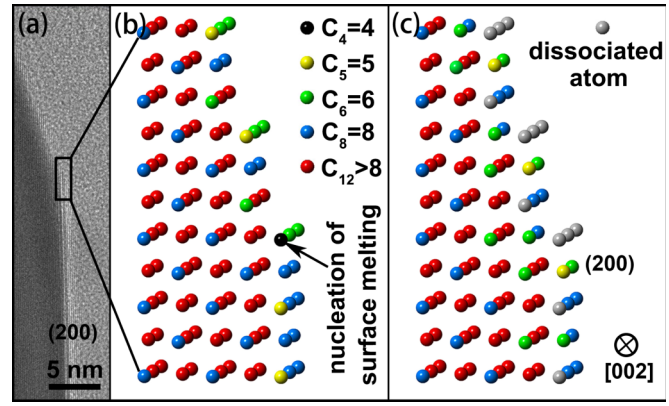

FIG. 3. Surface-melting nucleation model of the edge and corner of the Cu nanoparticle. (a) Corner and edge of the Cu nanoparticle. (b) Color coding of the initial states of the corner and edge atoms with different coordination numbers. (c) Nucleation state of the corner in the surface-melting process, in which gray balls are the melted atoms and the coordination numbers of the other atoms change as surface melting proceeds.

During the heating process, the atom with the lowest coordination number ($C_i = 4$) at the edge and corner first melts [Fig. 3(b)]. Subsequently, the atoms with coordination numbers of 5 and 6 separate from their lattice positions [gray balls in Fig. 3(c)] and form the nucleated region Q_1 [Fig. 2(b)] (Lindemann criterion [42]). Surface melting occurs until the nucleated region reaches critical size Q_2 [Fig. 2(c)]. At this time, the nucleus no longer increases in the depth direction owing to the negative curvature of the surface constraints, and collapse melting occurs along the Cu(200) surface.

MD simulations of the Nb(110) surface-melting process show that at high temperatures, the internal energy of each Nb(110) surface atomic layer decreases with increasing number of layers until the 10th layer [43,44]. This means that the melting process of the atomic layers within ten layers of the surface is less affected by surface melting. In this work, for the Cu(200) surface, melting after the 15th layer is less affected by surface melting. To understand the mechanism at the atomic scale, the Cu(200) surface structural evolution curves during the melting process at 1000 K by MD were obtained (Fig. 4) [15]. According to the results, it is possible that multiple layers of Cu(200) simultaneously melt, which is mainly because the melting range is different for each layer [44]. For example, at 700 ps, the atoms within the first seven layers have completely melted and the atoms farther than seven layers away remain crystalline. At 800 ps, the atoms within 14 layers have completely melted and the atoms farther than 14 layers away remain crystalline. At 900 ps, 20 layers of atoms have completely melted (Fig. 4). If the sample is affected by external factors at 800 ps, such as electron beam perturbation, small temperature fluctuations, and other factors, the atoms of the first 14 layers first melt from the edge and corner and then rapidly spread to the other end and melt to become liquid (the liquid is barely visible in the TEM owing to problems, such as contrast). The Cu crystal surface is then refreshed and

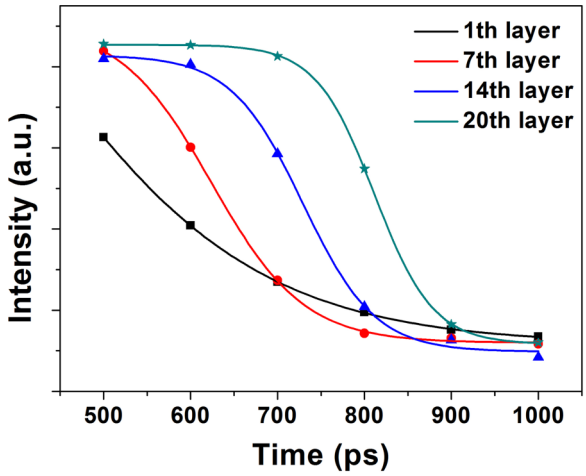

FIG. 4. Structural evolution of the different layers of the Cu(200) surface during the melting process at 1000 K. The data were obtained by collecting the intensity values of the first peak of the radial distribution functions.

this melting process is repeated. Because melting of the Cu nanoparticle begins at the edge and corner, multiple layers, such as the 14 layers in Fig. 2, might simultaneously melt and disappear because of the unfavorable internal energy [43].

We will briefly discuss the relation between the melting point of Cu nanoparticles and their morphology. According to this work, the surface-melting temperature of Cu nanoparticles is associated with the edge and corner structure. According to the present simulations, the melting temperature is also related to the crystal face. A high-index surface usually has a lower melting temperature. The melting temperature of the

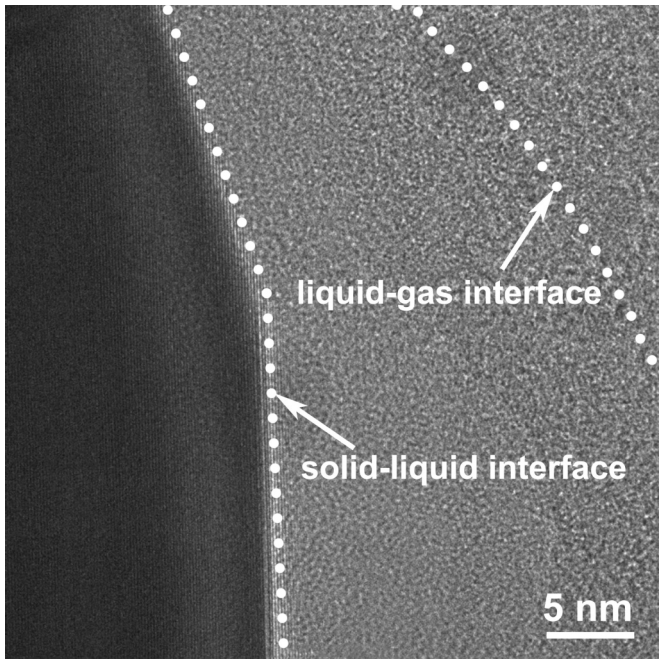

FIG. 5. The surface of the Cu nanoparticle was covered by the liquid film at 750°C, in which the solid-liquid interface and the liquid-gas interface are shown.

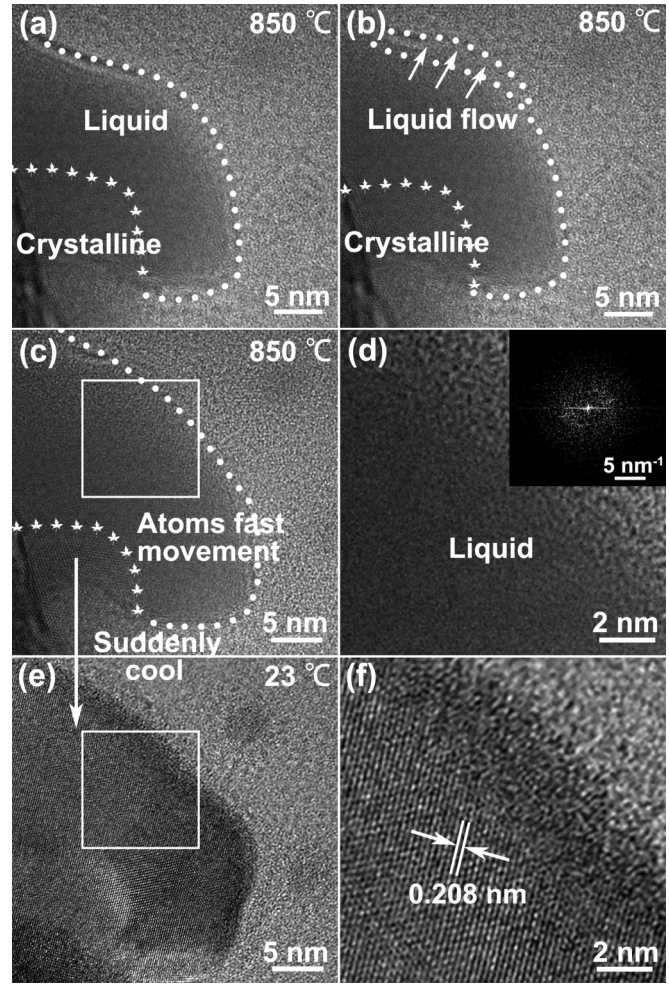

FIG. 6. Liquid film on the surface of the Cu nanoparticle. (a)–(c) TEM bright-field images at 850°C. (d) Enlarged image of the box region in (c) and its FFT pattern. (e) TEM bright-field image at 23°C. (f) Enlarged image of the box region in (e).

Cu(111) surface is 1083°C, whereas calculations show that the melting temperature of the Cu(200) surface is 967 ± 25°C [17]. Experiments show that the melting temperatures of 40 and 50 nm Cu nanoparticles are about 187 and 327°C, respectively [24]. Because the surface of these nanoparticles has a lot of low cohesive energy structures, such as edges and corners or high-index surfaces, their melting temperature is much lower than that of the bulk Cu. Therefore, to avoid high-temperature failure, Cu nanomaterials should be prepared with less edges and corners, and more exposed (111) surface.

It should be noted that the observations in this study could also be caused by volatilization of Cu nanoparticles. To exclude this possibility, additional analyses and experiments were performed. As shown in Video S1 in the SM [29], the atoms near the surface of the Cu nanoparticle move faster than those in the remote regions. The speed of an atom is directly correlated to its state. A liquid film may exist around the Cu nanoparticle. There is a solid-liquid interface and a liquid-gas interface in the sample (Fig. 5). Therefore, the surface of the Cu nanoparticle first changes from solid to liquid (surface-melting

phenomenon) and then evaporation from the liquid state to the gaseous state occurs.

To confirm this hypothesis, we performed additional experiments to prove that the state of Cu near the solid surface is liquid. The Cu nanoparticle was heated to 850°C. A liquid film will more easily form on the Cu nanoparticle at this temperature than at 750°C. Figures 6(a)–6(c) show that there is a clear liquid film near the Cu crystal at 850°C. Compared with Fig. 6(a), the liquid film [Fig. 6(b)] will flow outward, and the flow of the liquid film continues as time proceeds [Fig. 6(c)], as shown in Video S3 in the SM [29]. It is interesting that the movement of the atoms in the liquid film is faster than those of Si_3N_4. The process is shown in Video S4 in the SM [29]. An enlarged image and the box region in Fig. 6(c) and its FFT pattern are shown in Fig. 6(d).

The sample was then suddenly cooled to 23°C, resulting in the liquid film recrystallizing as a solid [Fig. 6(e)]. Figure 6(f) shows an enlarged image of the square region in Fig. 6(e), which indicates that the sample is crystalline. From comparison of Figs. 6(c) and 6(e), the farther away from the crystalline Cu surface, the poorer the visibility of the liquid state, which means that the liquid film is thinner. Conversely, the thickness of the Cu nanoparticle in Video S1 is larger than that in Videos S3 and S4 in the SM [29], and the visibility is poorer because of the poor contrast of the liquid. Thus, it is concluded that a liquid film exists near the Cu nanoparticle where the atoms move very fast. Therefore, the observation in this study is melting rather than evaporation.

Surface melting of Cu nanoparticles can be affected by a number of factors, such as microscopic strain, electron beam damage, and so forth. To confirm the conclusions of this study and exclude some of these factors, we will discuss the factors in the following paragraph.

There is large microscopic strain when the sample is prepared by mechanical alloying. However, this microscopic strain will be eliminated after high-temperature heat treatment and thermal reduction [45,46]. Moreover, the Cu nanoparticle crystallinity is good and no obvious defects are observed by high-resolution *in situ* TEM at high temperature. Therefore, we believe that surface melting is hardly affected by internal stress. Electron beam damage of the sample mainly originates from three sources: radiolysis, heating, and knock-on damage or sputtering [47]. For metallic Cu particles, the atoms are bound by strong metal bonds, so there is no obvious radiation damage. For metals and other good conductors, electron beam heating is negligible under standard TEM conditions. Thus, the surface-melting temperature of Cu mainly comes from the heating chip. The Talos F200X transmission electron microscope (FEG source, electron beam energy of 200 keV) can avoid the effects of hot electrons and the energy is not large enough to cause the Cu atoms to shift [47].

IV. CONCLUSION

The surface-melting process of Cu(200) at 750°C has been observed at the atomic scale by *in situ* TEM. Surface-melting nucleation first occurs at the edge and corner of the Cu(200) surface. Subsequently, the size of the nucleus increases to a critical size (about 14 layers). Finally, collapse-type expansion melting of the 14 layers rapidly extends to the whole Cu(200) surface. This surface-melting process repeatedly occurs. This work reveals that the main origin of surface melting of nanoparticles is the edge and corner structure where atoms have low cohesive energy, rather than the vacancies on the flat surface.

ACKNOWLEDGMENTS

We thank Jie Xu and Haoxuan Liu for useful discussion, Yajiao Huo for assistance with sample preparation, and Xianyun Peng for assistance with writing the manuscript. This work was financially supported by the National Natural Science Foundation of China (Grants No. 21603161 and No. 51671145), the National Program for Thousand Young Talents of China, the Tianjin Municipal Education Commission, the Tianjin Municipal Science and Technology Commission (Grant No. 15JCYBJC52600), and the Fundamental Research Fund of Tianjin University of Technology.

[1] F. W. D. Wette, *Solvay Conference on Surface Science* (Springer-Verlag, Berlin, 1988).
[2] E. T. Chen, R. N. Barnett, and U. Landman, Phys. Rev. B: Condens. Matter **41**, 439 (1990).
[3] R. W. Cahn, Nature (London) **323**, 668 (1986).
[4] K. Lu and Z. H. Jin, Curr. Opin. Solid State Mater. Sci. **5**, 39 (2001).
[5] H. Reiss and I. B. Wilson, J. Colloid Sci. **3**, 551 (1948).
[6] D. Nenow and A. Trayanov, J. Cryst. Growth **99**, 102 (1990).
[7] P. Bavli, E. Polturak, and J. Adler, Phys. Rev. B **84**, 235442 (2011).
[8] G. Bilalbegovic, Phys. Rev. B **55**, 16450 (1997).
[9] B. Pluis, A. W. Denier van der Gon, J. W. M. Frenken, and J. F. van der Veen, Phys. Rev. Lett. **59**, 2678 (1987).
[10] P. Carnevali, F. Ercolessi, and E. Tosatti, Phys. Rev. B: Condens. Matter **36**, 6701 (1987).
[11] H. M. V. Pinxteren and J. W. M. Frenken, Surf. Sci. **275**, 383 (1992).
[12] Y. Cao and E. Conrad, Phys. Rev. Lett. **65**, 2808 (1990).
[13] G. Bilalbegović and E. Tosatti, Phys. Rev. B: Condens. Matter **48**, 11240 (1993).
[14] L. Pedemonte, G. Bracco, R. Beikler, E. Taglauer, A. Robin, and W. Heiland, Surf. Sci. **532**, 13 (2003).
[15] P. Stoltze, J. K. Nørskov, and U. Landman, Phys. Rev. Lett. **61**, 440 (1988).
[16] P. Stoltze, J. K. Nørskov, and U. Landman, Surf. Sci. **220**, L693 (1989).
[17] H. Häkkinen and M. Manninen, Phys. Rev. B: Condens. Matter **46**, 1725 (1992).
[18] H. Häkkinen and U. Landman, Phys. Rev. Lett. **71**, 1023 (1993).
[19] J. Merikoski, H. Häkkinen, M. Manninen, J. Timonen, and K. Kaski, Phys. Rev. B: Condens. Matter **49**, 4938 (1994).

[20] F. L. Tang, X. G. Cheng, W. J. Lu, and W. Y. Yu, Physica B **405**, 1248 (2009).
[21] M. Polcik, L. Wilde, and J. Haase, Phys. Rev. Lett. **78**, 491 (1997).
[22] M. B. Gawande, A. Goswami, F. X. Felpin, T. Asefa, X. Huang, R. Silva, X. Zou, R. Zboril, and R. S. Varma, Chem. Rev. **116**, 3722 (2016).
[23] F. Delogu, Phys. Rev. B **72**, 205418 (2005).
[24] Oleg A. Yeshchenko, Igor M. Dmitruk, Alexandr A. Alexeenko, and Andriy M. Dmytruk, Phys. Rev. B **75**, 085434 (2007).
[25] D. Chen, J. Alloys Compd. **504**, S345 (2010).
[26] F. Niekiel, S. M. Kraschewski, J. Müller, B. Butz, and E. Spiecker, Ultramicroscopy **176**, 161 (2016).
[27] S. Plimpton, J. Comput. Phys. **117**, 1 (1995).
[28] M. S. Daw and M. I. Baskes, Phys. Rev. B: Condens. Matter **29**, 6443 (1984).
[29] See Supplemental Material at http://link.aps.org/supplemental/10.1103/PhysRevB.98.045425 for the Videos S1–S4 and Figs. S1– S3.
[30] W. Humphrey, A. Dalke, and K. Schulten, J. Mol. Graphics **14**, 33 (1996).
[31] V. P. Skripov, V. P. Koverda, and V. N. Skokov, Phys. Status Solidi A **66**, 109 (1981).
[32] H. Reiss, P. Mirabel, and R. L. Whetten, J. Phys. Chem. **92**, 7241 (1988).
[33] R. R. Vanfleet and J. M. Mochel, Surf. Sci. **341**, 40 (1995).
[34] G. Ouyang, C. X. Wang, and G. W. Yang, Chem. Rev. **109**, 4221 (2009).
[35] B. J. Siwick, J. R. Dwyer, and R. E. Jordan, Science **302**, 1382 (2003).
[36] W. H. Qi, B. Y. Huang, M. P. Wang, Z. Li, and Z. M. Yu, Phys. Lett. A **370**, 494 (2007).
[37] M. A. Shandiz, A. Safaei, S. Sanjabi, and Z. H. Barber, Solid State Commun. **145**, 432 (2008).
[38] J. Zhong, L. H. Zhang, Z. H. Jin, M. L. Sui, and K. Lu, Acta Mater. **49**, 2897 (2001).
[39] S. Link, C. Burda, B. Nikoobakht, and M. A. Elsayed, J. Phys. Chem. B **104**, 6152 (2000).
[40] A. V. Simakin, V. V. Voronov, G. A. Shafeev, R. Brayner, and F. Bozon-Verduraz, Chem. Phys. Lett. **348**, 182 (2001).
[41] R. Shidpour, H. H. Delavari, and M. Vossoughi, Chem. Phys. **378**, 14 (2010).
[42] C. Chakravarty, P. G. Debenedetti, and F. H. Stillinger, J. Chem. Phys. **126**, 204508 (2007).
[43] X. Yang, W. Hu, and Z. Zhang, Curr. Appl. Phys. **10**, 436 (2010).
[44] X. Y. Yang and W. Dan, Appl. Surf. Sci. **256**, 3197 (2010).
[45] F. Popa, I. Chicinaş, O. Isnard, and V. Pop, J. Therm. Anal. Calorim. **110**, 295 (2012).
[46] V. Pop, O. Isnard, and I. Chicinaş, J. Alloys Compd. **361**, 144 (2003).
[47] D. B. Williams and C. B. Carter, *Transmission Electron Microscopy: A Textbook for Materials Science* (Springer, New York, 2009).